Title

New Limit for Neutrinoless Double-Beta Decay of Mo100 from the CUPID-Mo Experiment

Journal

Physical Review Letters, 126(18)

ISSN

0031-9007

Authors

Armengaud, E

Augier, C

Barabash, AS

et al.

Publication Date

2021-05-07

DOI

10.1103/physrevlett.126.181802

Peer reviewed

A new limit for neutrinoless double-beta decay of ^{100}Mo from the CUPID-Mo experiment

(CUPID-Mo Collaboration)

E. Armengaud,[1] C. Augier,[2] A. S. Barabash,[3] F. Bellini,[4,5] G. Benato,[6] A. Benoît,[7] M. Beretta,[8] L. Bergé,[9] J. Billard,[2] Yu. A. Borovlev,[10] Ch. Bourgeois,[9] V. B. Brudanin,[11] P. Camus,[7] L. Cardani,[5] N. Casali,[5] A. Cazes,[2] M. Chapellier,[9] F. Charlieux,[2] D. Chiesa,[12,13] M. de Combarieu,[14] I. Dafinei,[5] F. A. Danevich,[15] M. De Jesus,[2] T. Dixon,[8] L. Dumoulin,[9] K. Eitel,[16] F. Ferri,[1] B. K. Fujikawa,[17] J. Gascon,[2] L. Gironi,[12,13] A. Giuliani,[9,*] V. D. Grigorieva,[10] M. Gros,[1] E. Guerard,[9] D. L. Helis,[1] H. Z. Huang,[18] R. Huang,[8] J. Johnston,[19] A. Juillard,[2] H. Khalife,[9] M. Kleifges,[20] V. V. Kobychev,[15] Yu. G. Kolomensky,[8,17] S.I. Konovalov,[3] A. Leder,[19] P. Loaiza,[9] L. Ma,[18] E. P. Makarov,[10] P. de Marcillac,[9] R. Mariam,[9] L. Marini,[8,17,6] S. Marnieros,[9] D. Misiak,[2] X.-F. Navick,[1] C. Nones,[1] E. B. Norman,[8] V. Novati,[9,†] E. Olivieri,[9] J. L. Ouellet,[19] L. Pagnanini,[21,6] P. Pari,[14] L. Pattavina,[6,22] B. Paul,[1] M. Pavan,[12,13] H. Peng,[23] G. Pessina,[13] S. Pirro,[6] D. V. Poda,[9] O. G. Polischuk,[15] S. Pozzi,[13] E. Previtali,[12,13] Th. Redon,[9] A. Rojas,[24] S. Rozov,[11] C. Rusconi,[25] V. Sanglard,[2] J. A. Scarpaci,[9] K. Schäffner,[6] B. Schmidt,[17,†] Y. Shen,[18] V. N. Shlegel,[10] B. Siebenborn,[16] V. Singh,[8] C. Tomei,[5] V. I. Tretyak,[15] V. I. Umatov,[3] L. Vagneron,[2] M. Velázquez,[26] B. Welliver,[17] L. Winslow,[19] M. Xue,[23] E. Yakushev,[11] M. Zarytskyy,[15] and A. S. Zolotarova[9]

[1] *IRFU, CEA, Université Paris-Saclay, F-91191 Gif-sur-Yvette, France*
[2] *Univ Lyon, Université Lyon 1, CNRS/IN2P3, IP2I-Lyon, F-69622, Villeurbanne, France*
[3] *National Research Centre Kurchatov Institute, Institute of Theoretical and Experimental Physics, 117218 Moscow, Russia*
[4] *Dipartimento di Fisica, Sapienza Università di Roma, P.le Aldo Moro 2, I-00185, Rome, Italy*
[5] *INFN, Sezione di Roma, P.le Aldo Moro 2, I-00185, Rome, Italy*
[6] *INFN, Laboratori Nazionali del Gran Sasso, I-67100 Assergi (AQ), Italy*
[7] *CNRS-Néel, 38042 Grenoble Cedex 9, France*
[8] *University of California, Berkeley, California 94720, USA*
[9] *Université Paris-Saclay, CNRS/IN2P3, IJCLab, 91405 Orsay, France*
[10] *Nikolaev Institute of Inorganic Chemistry, 630090 Novosibirsk, Russia*
[11] *Laboratory of Nuclear Problems, JINR, 141980 Dubna, Moscow region, Russia*
[12] *Dipartimento di Fisica, Università di Milano-Bicocca, I-20126 Milano, Italy*
[13] *INFN, Sezione di Milano-Bicocca, I-20126 Milano, Italy*
[14] *IRAMIS, CEA, Université Paris-Saclay, F-91191 Gif-sur-Yvette, France*
[15] *Institute for Nuclear Research of NASU, 03028 Kyiv, Ukraine*
[16] *Karlsruhe Institute of Technology, Institute for Astroparticle Physics, 76021 Karlsruhe, Germany*
[17] *Lawrence Berkeley National Laboratory, Berkeley, California 94720, USA*
[18] *Key Laboratory of Nuclear Physics and Ion-beam Application (MOE), Fudan University, Shanghai 200433, PR China*
[19] *Massachusetts Institute of Technology, Cambridge, MA 02139, USA*
[20] *Karlsruhe Institute of Technology, Institute for Data Processing and Electronics, 76021 Karlsruhe, Germany*
[21] *INFN, Gran Sasso Science Institute, I-67100 L'Aquila, Italy*
[22] *Physik Department, Technische Universität München, Garching D-85748, Germany*
[23] *Department of Modern Physics, University of Science and Technology of China, Hefei 230027, PR China*
[24] *LSM, Laboratoire Souterrain de Modane, 73500 Modane, France*
[25] *Department of Physics and Astronomy, University of South Carolina, SC 29208, Columbia, USA*
[26] *Université Grenoble Alpes, CNRS, Grenoble INP, SIMAP, 38402 Saint Martin d'Héres, France*

(Dated: November 30, 2020)

The CUPID-Mo experiment at the Laboratoire Souterrain de Modane (France) is a demonstrator for CUPID, the next-generation ton-scale cryogenic $0\nu\beta\beta$ experiment. It consists of a 4.2 kg array of 20 enriched $Li_2{}^{100}MoO_4$ scintillating bolometers to search for the lepton number violating process of $0\nu\beta\beta$ decay in ^{100}Mo. With more than one year of operation (2.16 kg×yr of physics data), no event in the region of interest and hence no evidence for $0\nu\beta\beta$ is observed. We report a new limit on the half-life of $0\nu\beta\beta$ decay in ^{100}Mo of $T_{1/2} > 1.5 \times 10^{24}$ yr at 90% C.I. The limit corresponds to an effective Majorana neutrino mass $\langle m_{\beta\beta}\rangle < (0.3\text{–}0.5)$ eV, dependent on the nuclear matrix element in the light Majorana neutrino exchange interpretation.

The discovery that neutrinos are massive particles through the evidence of neutrino flavor oscillations [1] opens the question of neutrino mass generation. Instead of having Dirac nature as charged leptons and quarks, the scale of neutrino masses could be well motivated by the Majorana theory [2, 3]. In this scenario neutrinos could coincide with their antimatter partner [4, 5] which

* e-mail: andrea.giuliani@IJCLab.in2p3.fr
† Now at: Northwestern University, Evanston, IL 60208, USA

would have a tremendous impact on our vision of Nature, implying the violation of the total lepton number L as well as for the matter-antimatter asymmetry in the Universe [6], see also review [7].

The distinction between Dirac and Majorana behavior is an extreme experimental challenge. Neutrinoless double-beta ($0\nu\beta\beta$) decay is the traditional and the most sensitive tool to probe the Majorana nature of neutrinos. This process is a nuclear transition consisting in the transformation of an even-even nucleus into a lighter isobar containing two more protons and accompanied by the emission of two electrons and no other particles, with a change of the lepton number L by two units [8–11]. An observation of this rare process would establish that neutrinos are Majorana particles [12]. The current most stringent limits on $0\nu\beta\beta$ decay half-lifes are at the level of 10^{26} yr in ^{136}Xe and ^{76}Ge [13, 14].

$0\nu\beta\beta$ decay can be induced by a variety of mechanisms [9, 11, 15, 16]. Among them, the so-called mass mechanism — consisting in the exchange of a virtual light Majorana neutrino — represents a minimal extension of the Standard Model. In this mechanism, the $0\nu\beta\beta$ decay rate is proportional to the square of the effective Majorana neutrino mass $\langle m_{\beta\beta}\rangle$, a linear combination of the three neutrino mass eigenvalues which fixes the absolute neutrino mass scale. Present limits on $\langle m_{\beta\beta}\rangle$ are in the range of $(0.06 - 0.6)$ eV [11], assuming that the axial charge g_A is not quenched and equal to the free nucleon value of $\simeq 1.27$ [17–19].

The distinctive signal of $0\nu\beta\beta$ decay is a peak in the total energy spectrum of the two emitted electrons at the total available energy $Q_{\beta\beta}$ of the $0\nu\beta\beta$ transition, enlarged only by the finite detector energy resolution. Besides $0\nu\beta\beta$ decay, candidate nuclei undergo standard two-neutrino double-beta ($2\nu\beta\beta$) decay where two anti-neutrinos are emitted along with the two electrons [20]. $2\nu\beta\beta$ conserves the lepton number L and as anti-neutrinos escape detection, the two-electron energy spectrum is a continuum extending from zero to $Q_{\beta\beta}$. This process has been observed in several nuclei with half-lives in the 10^{18}–10^{24} yr range [21, 22]. Among the 35 natural double-beta emitters [23], only a few of them are experimentally relevant because of their high $Q_{\beta\beta}$ (> 2 MeV) with high decay probability, typically favorable backgrounds at higher energy and their high natural isotopic abundance and/or technically feasible isotopic enrichment.

Low-temperature calorimeters, often named bolometers, are the detectors of choice for several experimental efforts, including the one reported here. Featuring high energy resolution, high efficiency, and flexibility in detector-material choice [24–26], bolometers are perfectly tailored to $0\nu\beta\beta$ search. These detectors consist in a single crystal that contains the $0\nu\beta\beta$ source coupled to a temperature sensor. The signal is collected at very low temperatures $\lesssim 20$ mK for large (0.1–1 kg) bolometers and consists of a thermal pulse registered by the sensor.

A detector embedding a candidate with $Q_{\beta\beta} > 2615$ keV is an optimal choice in terms of background control, as the bulk of the γ natural radioactivity ends at 2615 keV, corresponding to the energy of the ^{208}Tl line in the ^{232}Th decay chain. However, the energy region above ~ 2.6 MeV is dominated by events due to surface radioactive contamination, especially energy-degraded α particles [27, 28], as shown by the results of CUORE, the largest $0\nu\beta\beta$ bolometric experiment currently under way.

A method to reject α events in bolometers exploits light emission — scintillation or Cherenkov — from certain detector materials [25, 26, 29–34]. Since the γ and β light yield is appreciably different from the α light yield at equal deposited energy, while the bolometric thermal response is almost equivalent, the simultaneous detection of light and heat can effectively reject the surface α background.

The detector technology of CUPID-Mo has been developed by the LUMINEU Collaboration [35, 36] and is described together with the experimental setup in [37]. The isotope of interest ^{100}Mo features a $Q_{\beta\beta}$ of (3034.40±0.17) keV [38] and a natural abundance of 9.7% making large scale enrichment viable by gas centrifuge isotopic separation. In CUPID-Mo, it is embedded into scintillating $Li_2{}^{100}MoO_4$ (LMO) crystals by a double low-thermal-gradient Czochralski crystallization process [39] from enriched Mo previously used in the NEMO-3 experiment [40]. A total of twenty cylindrical ~ 210 g crystals are stacked into 5 towers which results in a ^{100}Mo mass of (2.258 ± 0.005) kg with an average ^{100}Mo isotopic abundance of (96.6 ± 0.2)%. Bolometric Ge light detectors (LDs) complement each LMO detector module, such that all but the top LMO elements of the 4-crystal tower see a LD at both the top and bottom. The LMO crystals as well as the LDs are instrumented with Neutron-Transmutation-Doped (NTD)-Ge sensors [41]. The towers are installed with a mechanical decoupling inside the EDELWEISS cryogenic infrastructure [42, 43] at the Laboratoire Souterrain de Modane in France.

The data of the present analysis have been acquired over a 380 day period between March 2019 and April 2020 at operation temperatures of 20.7 and 22 mK. 82 % of the time was devoted to the $0\nu\beta\beta$ search, split into 240 days of physics data and 73 days of calibration data.

We only consider 213 out of the 240 days of physics data, split into 7 datasets for which we also have calibration data with high statistics and hence a precise knowledge of the energy scale.

We further exclude periods of temperature instabilities, disturbances in the underground laboratory and periods of excessive noise on the individual detectors reducing the physics exposure by 6%. We reject one of the twenty LMO bolometers that shows an abnormal performance [37] and obtain a physics exposure of 2.16 kg×yr ($Li_2{}^{100}MoO_4$).

All data are acquired as a continuous stream with 500 Hz sampling frequency and analyzed with a software package developed by the CUORE [44] and CUPID-0

[45] Collaborations, first used in CUPID-Mo in [37, 46]. We use an optimum filter based analysis chain with 3 s long pulse traces for both the LMO and LD channels. The data were re-triggered offline using the optimum filter [28, 47]. This resulted in significantly lower trigger thresholds with 90% efficiency values attained at typical (median) energies of 9.4 keV / 0.5 keV for the LMOs / LDs. The LMOs analysis and coincidence thresholds have been set at 45 keV, well above this efficiency turn on. For each signal on an LMO detector we evaluate the resolution weighted average light signal of the two (one) adjacent LDs to discriminate α events, exhibiting $\sim$20% of the light yield of $\gamma\&\beta$ events of the same energy [37]. Furthermore, the energy difference of the upper and lower LDs, corrected for geometrical light collection efficiencies is computed to extend the identification of near surface decays. We developed a new pulse shape analysis procedure for the signal of the LMO detector to remove remaining spikes and pulser-induced cross-talk events from the data. As described in detail in [48] a principal component analysis (PCA) is used to establish a characteristic shape of a pulse as the leading PCA component(s). We then compute the reconstruction error defined as the square-root of the variance from a pulse with respect to its projection onto the leading PCA component(s). The reconstruction error shows a linear energy dependence and a constant spread over our $\gamma\&\beta$ data which makes it ideally suitable for the $0\nu\beta\beta$ analysis where it needs to be extrapolated to $Q_{\beta\beta}$ of ^{100}Mo at 3034 keV. Together with this very simple energy dependence we gain a $\sim$ 9% efficiency increase compared to the analysis presented in [46]. Lastly we calibrate the response of the LMO detectors with a 2nd order polynomial using the U/Th calibration data as in [46] and cross-calibrate the LD against the LMO signals.

We adopt a blinding strategy removing all events in a $\pm$50 keV window around $Q_{\beta\beta}$ to avoid any bias in the optimization of our analysis procedures and consider the following event selections. For events

- to be contained in a single crystal and in anti-coincidence with a triple module trigger and energy deposit in the muon-veto system [49] based on a 100 ms time window;
- to have a single trigger in each 3-s pulse window;
- to have a flat pre-trace with a slope of less than 15 median absolute deviations;
- to have a pulse shape compatible with the principal components established by the PCA. This cut is optimized using calibration data by maximizing a hypothetical discovery sensitivity for a $0\nu\beta\beta$ process equal in half-live to the previous best limit [40], see also [48];
- to have the expected light yield for $\gamma\&\beta$ events and no difference in top and bottom LDs. Both of these cuts are set to obtain close to full coverage at $\pm 3\,\sigma$ each, based on a Gaussian fit of the light yield in calibration data. The energy dependence of the cut was modeled with a linear function after we observed an excess broadening of the recorded light yield with respect to the photon statistics model discussed in [37]. The excess width is associated with an under-sampling of the faster LD pulses and is presently under further investigation.

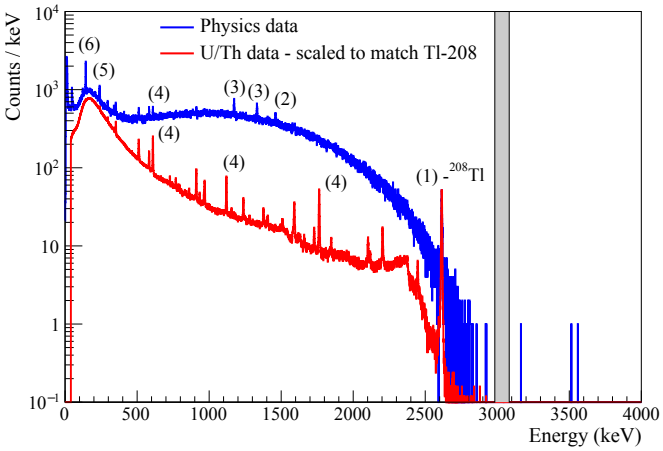

FIG. 1. Physics spectrum (blue) for 2.16 kg×yr of data and calibration spectrum (red) scaled to match the 2615 keV counts from ^{208}Tl. A $\pm$50 keV region around $Q_{\beta\beta}$ has been blinded (gray). The most prominent γ-peaks in the physics and calibration data are the following: (1) ^{208}Tl 2615 keV, (2) ^{40}K 1461 keV, (3) ^{60}Co 1173 and 1332 keV, (4) ^{214}Bi 1764, 1120 and 609 keV, (5) ^{212}Pb 239 keV, (6) ^{99}Mo 142 keV.

The resulting spectra summed over 19 LMO detectors and the entire data taking period are shown in Fig. 1.

The physics data exhibit an extended $2\nu\beta\beta$ component, associated with the short $2\nu\beta\beta$ half-life (high rate) of ^{100}Mo [50, 51], which dominates the spectrum from 0.5 to 3 MeV. Above this component only a limited number of γ peaks from remaining natural radioactivity in the experimental setup are visible. The most prominent γ peaks in our data are ^{208}Tl, ^{40}K, ^{60}Co and an activation γ peak from ^{99}Mo, visible for a short time after a neutron irradiation of the detectors. For more details we refer to a prior characterization of the backgrounds in this setup by the EDELWEISS Collaboration in [42]. The four labeled γ peaks in the scaled calibration spectrum in Fig. 1 are used for the calibration of each data-set.

We optimize the $0\nu\beta\beta$ search window for a Poisson counting process in the low background regime. We consider the current exposure of 2.16 kg×yr as a first unblinding of the full data of the now completed CUPID-Mo experiment. For the definition of the signal region of interest (ROI) we hence optimize using the full expected exposure and consider detector and data-set based resolutions and a preliminary background index evaluated from the current data release.

The detector resolutions are extracted from a data-set

based, simultaneous unbinned extended maximum likelihood fit of the ^{208}Tl 2615 keV peak in calibration data. The fit is performed with individual parameters for the detector resolutions, peak amplitudes and position and with common parameters for the peak-background ratio [46]. Limited by the statistics in physics data we estimate a global scaling factor (common to all data-sets and detectors) that is used to project the individual calibration resolutions to $Q_{\beta\beta}$. We report the more conservative value of an extrapolation considering the preferred scaling described in [46] as well as the polynomial fit used in [27, 28]. This results in a characteristic resolution of (7.6 ± 0.7) keV FWHM at $Q_{\beta\beta}$ for the overall data taking. We note that the estimation of the scaling factor does have some sensitivity to non-Gaussian tails in calibration data, leading to an excess systematic error of 2%.

The accuracy of the energy scale is further investigated based on the mean position of the 352, 583, 609, 1461 and 2615 keV peaks in our physics spectrum (Fig. 1). A 2nd order polynomial fit in reconstructed-to-expected peak position results in an energy bias at $Q_{\beta\beta}$ compatible with zero: $E_{bias}^{Q_{\beta\beta}} = (-0.2 \pm 0.4)$ keV. We note that we excluded the prominent peaks from ^{60}Co, due to a known spatial non-uniformity, and ^{99}Mo, due to its time dependence.

The background index has been evaluated from the still blinded data with a phenomenological fit model that contains an exponential to approximate both the high energy part of the $2\nu\beta\beta$ spectrum as well as tails from U/Th contaminants in the setup, and a constant as a conservative estimate for the coincident detection of two $2\nu\beta\beta$ events in the same crystal, remaining unvetoed muon events and close contamination from the high energy beta decays in the natural U/Th chains. The result of an unbinned extended maximum likelihood fit is strongly dependent on the initial and final fit range. For a fit with the start range varied from 2.65–2.9 MeV and the final fit range from the upper end of the blinded region to 4 MeV we obtain a background index of 2×10^{-3} counts/(keV×kg×yr) to 6×10^{-3} counts/(keV×kg×yr) in a 10 keV window around $Q_{\beta\beta}$. This background estimate is consistent with the results from a preliminary Geant4-based reconstruction of the $\gamma\&\beta$ backgrounds, similar to the ones described in [32, 52, 53].

Considering the large remaining uncertainty we round the background index for the ROI optimization to $b = 5 \times 10^{-3}$ counts/(keV×kg×yr). We model the background as locally flat, consider detector and data-set based resolutions, and simulate the $0\nu\beta\beta$ peak containment in our Geant4 Monte Carlo model. We maximize the mean limit setting sensitivity of a Poisson process

$$\overline{S_{90}} = \sum_{i=0}^{\infty} P(i,b) \cdot S_{90}(i)$$

with the sum running over the product of the Poisson probability $P(i,b)$ of obtaining i background events for a background index b times the expected 90% confidence exclusion limit $S_{90}(i)$. We transfer this maximization from the optimization of the energy range for a peak search in 19 (detectors) times 7 (data-sets) to the optimization of a single parameter by splitting the simulated smeared $0\nu\beta\beta$ peaks into 0.1 keV bins and ranking each bin associated with a triplet (detector, data-set, energy) in Signal-Background (B/S) likelihood space. The optimal cutoff parameter $(\mathrm{B/S})_{cutoff}$ results in a ROI that is on average (exposure weighted) 17.9 keV wide. It has a mean signal containment of 75.8% with a spread of ±1.0%. The ROI width corresponds to an average $2.7\,\sigma$ Gaussian coverage with the loss of $0\nu\beta\beta$ decay events in the full energy peak dominated by Bremsstrahlung loss from events close to the surface of the crystals. The optimization exhibits only a mild dependence on the background index or the knowledge of the resolution, with the overall containment changing by ±0.7% for a 50% change in b (2.2 keV wider, 1.5 keV narrower ROI). We truncate the computation of the mean limit setting sensitivity after the first three terms as the probability of 3 or more background events is negligible for the considered ROI.

We used two independent analyses to extract a limit or potential signal on the rate of $0\nu\beta\beta$ events. We present results from a likelihood analysis of the 100 keV wide blinded analysis region. This analysis has been implemented in the framework of the Bayesian Analysis Toolkit (BAT) [54], but we note that we obtained compatible results from a Poisson counting analysis. In the BAT analysis we consider both the signal region as well as the sidebands in our likelihood function

$$L = \prod_{i=1}^{3} \frac{e^{\lambda_i} \lambda_i^{n_i}}{n_i!},$$

which is the product over three Poisson terms with observed events n_i and expected events λ_i. The mean number of expected events λ_i is computed considering the phenomenological background model described above and a Gaussian signal contribution in which we leave the strength of the signal and flat background component free by using uninformative flat priors. After defining all analysis steps we unblind and obtain the spectrum in Fig. 2. We observe no event in the signal region and a single event (cyan) in the right-hand side region. The corresponding marginalized posterior distribution for the number of signal events has a most probable value of zero with an upper limit of 2.4 events at 90% C.I., resulting in a half-life limit for $0\nu\beta\beta$ decay in ^{100}Mo of $T_{1/2}^{0\nu} > 1.4 \times 10^{24}$ yr (90% C.I.). The posterior for the flat background is non-zero with a $1\,\sigma$ interval of $3^{+7}_{-3} \times 10^{-3}$ counts/(keV×kg×yr) and the posterior distributions for the parameters of the exponential are compatible with priors from a fit of the $2\nu\beta\beta$ spectrum in the 2650–2980 keV interval. We repeat the same fit for the approximation of a Gaussian signal with a locally flat background over the 100 keV analysis region. The limit

on $0\nu\beta\beta$ decay of ^{100}Mo is unaffected.

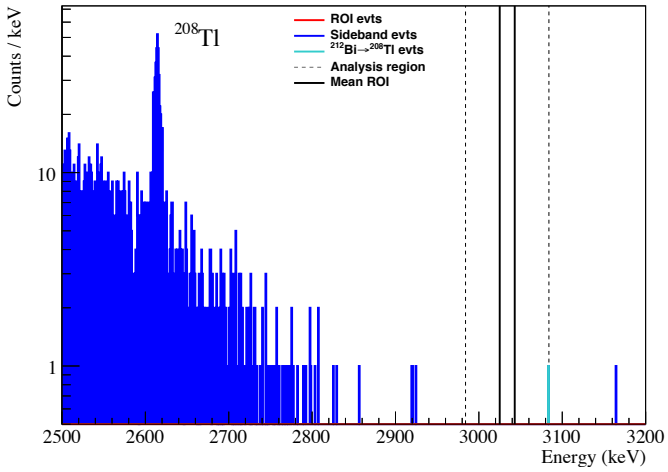

FIG. 2. Physics spectrum for 2.16 kg×yr of data after unblinding. No event is observed in the detector and dataset based ROI. A single event, highlighted in cyan has been observed in the analysis region. In a further refinement of the analysis it was identified as a β-candidate out of the ^{212}Bi→^{208}Tl→^{208}Pb part of the natural decay chain (see text). For visualization the exposure weighted mean ROI for $0\nu\beta\beta$ decay (17.9 keV wide) has been indicated with solid black lines.

TABLE I. Nuisance parameters included in the analysis and their implementation with Flat or Gaussian prior in the Bayesian fit. Parameters 2 and 5 are multiplicative scaling factors instead of absolute uncertainties, see text for details.

Systematic	Index	Value	Prior
Isotopic enrichment	1	0.966 ± 0.002	Gauss
$0\nu\beta\beta$ containment MC	2	1.000 ± 0.015	Gauss
$0\nu\beta\beta$ cont. detector response	3	0.95–1.00	Flat
Analysis efficiency [a]	4	0.906 ± 0.004	Gauss
Light yield selection [a]	5	0.998–1.008	Flat

[a] Data-set dependent; exposure weighted mean value presented.

Nuisance parameters are summarized in Table I. Uncertainties on the detector response, in particular the energy scale and resolutions, are included in the simulation of $0\nu\beta\beta$ events. They are hence covered in the resulting containment in the optimized central ROI on a detector and data-set basis and not considered independently. The only remaining uncertainty for the detector response (Index 3) is based on a potential non-gaussianity of the $0\nu\beta\beta$ peak. In this analysis we estimate this contribution based on the shape of the 2615 keV calibration peak. We observe evidence for non-gaussian tails, which are dominated by unrejected pile-up events caused by the high trigger-rate in calibration data. Given the much lower trigger-rate in physics data we believe that the containment reduction of up to 5%, obtained for pulse shape cuts that are representative of the ones used in physics data, is a very conservative estimate.

The second nuisance parameter on the containment (Index 2) accounts for the Geant4 modeling uncertainty of Bremsstrahlung events. Reported accuracies for the Geant4 Bremsstrahlung production of a few MeV electrons in thick targets [55, 56] of ∼10% result in a systematic uncertainty in the containment of 1.5% for our crystal geometry, which we include as a multiplicative factor with a Gaussian prior.

The inclusion of the analysis efficiency

$$\epsilon = (90.6 \pm 0.4\,(\text{stat.})\,^{+0.8}_{-0.2}\,(\text{syst.}))\%$$

is split into two parts. For the evaluation of the mean value and its statistical uncertainty (Index 4), we make use of the two independent signals in the LDs and LMOs to evaluate cut efficiencies on a clean sample of signal events in the 1.3 MeV to 2 MeV $2\nu\beta\beta$ spectrum or from the ^{210}Po peak [46]. Energy independent cuts are evaluated directly from the ratio between passed and total events with binomial uncertainty. The pulse shape analysis efficiency is extracted from a linear fit extrapolated to $Q_{\beta\beta}$ in order to account for the energy dependence in the reconstruction error.

The systematic uncertainty associated with the excess broadening of the light yield cut has been evaluated considering either the applied linear cut and linear energy dependence or a modified statistical behavior with arbitrary a_0 where the width of the light yield band is $\sigma(E) = \sqrt{\sigma_0^2 + (a_0\sqrt{E})^2}$. The quantification with a set of pseudo-experiments results in a likely underestimate of the signal acceptance which is reflected in our limit setting as a multiplicative factor with uniform prior in 0.998–1.008 (Index 5). Lastly, we include the subdominant uncertainty in the number of ^{100}Mo atoms of 0.2% (Index 1). All of these nuisance parameters are considered in the limit of our blind analysis $T^{0\nu}_{1/2} > 1.4 \times 10^{24}$ yr (90% C.I.).

We further refined our analysis after unblinding, implementing a cut designed to reject high energy β events from the $^{212}\text{Bi}\xrightarrow{\alpha}{}^{208}\text{Tl} \xrightarrow{\beta} {}^{208}\text{Pb}$ branch in the thorium chain ($T^{^{208}\text{Tl}}_{1/2} = 183$ s, 5 MeV Q-value). Similar to previous analyses with scintillating bolometers [29, 32, 45] we tag ^{212}Bi α candidates with energies in the 6.0–6.3 MeV range, and veto any decay in the same crystal in a 10 half-life period (1832 s). This cut has a negligible impact on the life-time (0.02%) accidentally rejecting 2:10000 events, while being fully efficient in rejecting any tagged true $^{212}\text{Bi}\xrightarrow{\alpha}{}^{208}\text{Tl} \xrightarrow{\beta} {}^{208}\text{Pb}$ event. It rejects the event highlighted in cyan in Fig. 2. The energy of the preceding α candidate is consistent with the Q-value of ^{212}Bi within 10 keV and the time difference between the events is 113 s.

We report a final $0\nu\beta\beta$ limit that is 1.3% stronger and rounds to

$$T^{0\nu}_{1/2} > 1.5 \times 10^{24}\,\text{yr (90\% C.I.)}.$$

The posterior for the flat background of the bayesian fit

in this case is peaked at zero with a 90% C.I. of 1.1×10^{-2} counts/(keV×kg×yr).

We interpret the obtained half-life limit in the framework of light Majorana neutrino exchange using $g_A = 1.27$, phase space factors from [57, 58] and nuclear matrix element calculations from [59–66]. The resulting limit on the effective Majorana neutrino mass of $\langle m_{\beta\beta} \rangle$ <(0.3–0.5) eV is the fourth most stringent limit world wide, obtained with a modest ^{100}Mo exposure of 1.19 kg×yr. It is the leading constraint for ^{100}Mo, exceeding the previous best limit from NEMO-3 [40] by 30% with almost 30 times lower ^{100}Mo exposure. The technology of CUPID-Mo has proven that it can be operated reliably, reaches high efficiency for $0\nu\beta\beta$ search of 68.6% (containment × analysis efficiency) and a resolution of 0.11% (1σ) at $Q_{\beta\beta}$. Together with a preliminary estimate of the background in the ROI at the few 10^{-3} counts/(keV×kg×yr) level, this results in an excellent sensitivity to $0\nu\beta\beta$ decay for the present and future experiments. Further analyses will be focused on precisely reconstructing remaining backgrounds, comparing to the best reported background index for a cryogenic $0\nu\beta\beta$ search [32] and to optimally design and use the technology of the CUPID-Mo experiment in CUPID [67].

The help of the technical staff of the Laboratoire Souterrain de Modane and of the other participant laboratories is gratefully acknowledged. This work has been partially performed in the framework of the LUMINEU program, funded by ANR (France). This work was also supported by CEA and IN2P3, by P2IO LabEx with the BSM-Nu project, by Istituto Nazionale di Fisica Nucleare, the Russian Science Foundation (Russia), the National Research Foundation (Ukraine), the US Department of Energy (DOE) Office of Science, the DOE Office of Science, Office of Nuclear Physics, the National Science Foundation (USA), by the France-Berkeley fund, the MISTI-France fund, and by the Chateaubriand Fellowship of the Office for Science & Technology of the Embassy of France in the United States. Individuals have received support from the National Academy of Sciences of Ukraine and P2IO LabEx managed by the ANR (France). This work makes use of the DIANA data analysis software which has been developed by the Cuoricino, CUORE, LUCIFER, and CUPID-0 Collaborations.

[1] I. Esteban, M. C. Gonzalez-Garcia, A. Hernandez-Cabezudo, M. Maltoni, and T. Schwetz, J. High Energy Phys. **01**, 106 (2019).
[2] R. N. Mohapatra and G. Senjanović, Phys. Rev. Lett. **44**, 912 (1980).
[3] J. Schechter and J. W. F. Valle, Phys. Rev. D **22**, 2227 (1980).
[4] E. Majorana, Nuovo Cim. **14**, 171 (1937).
[5] G. Racah, Nuovo Cim. **14**, 322 (1937).
[6] M. Fukugita and T. Yanagida, Phys. Lett. B **174**, 45 (1986).
[7] S. Davidson, E. Nardi, and Y. Nir, Phys. Rept. **466**, 105 (2008).
[8] W. H. Furry, Phys. Rev. **56**, 1184 (1939).
[9] S. M. Bilenky and C. Giunti, Int. J. Mod. Phys. A **30**, 1530001 (2015).
[10] S. Dell'Oro, S. Marcocci, M. Viel, and F. Vissani, Adv. High Energy Phys. **2016**, 2162659 (2016).
[11] M. J. Dolinski, A. W. Poon, and W. Rodejohann, Annu. Rev. Nucl. Part. Sci. **69**, 219 (2019).
[12] J. Schechter and J. W. F. Valle, Phys. Rev. D **25**, 2951 (1982).
[13] A. Gando *et al.* (KamLAND-Zen Collaboration), Phys. Rev. Lett. **117**, 082503 (2016).
[14] M. Agostini *et al.*, Science **365**, 1445 (2019).
[15] F. F. Deppisch, M. Hirsch, and H. Päs, J. Phys. G **39**, 124007 (2012).
[16] W. Rodejohann, J. Phys. G **39**, 124008 (2012).
[17] J. Suhonen and J. Kostensalo, Front. in Phys. **7**, 29 (2019).
[18] P. Gysbers *et al.*, Nat. Phys. **15**, 428 (2019).
[19] F. Šimkovic, R. Dvornický, and D. Štefánik, EPJ Web Conf. **194**, 02002 (2018).
[20] M. Goeppert-Mayer, Phys. Rev. **48**, 512 (1935).
[21] R. Saakyan, Annu. Rev. Nucl. Part. Sci. **63**, 503 (2013).
[22] A. S. Barabash, Universe **6**, 159 (2020).
[23] V. I. Tretyak and Y. G. Zdesenko, At. Data Nucl. Data Tables **80**, 83 (2002).
[24] E. Fiorini and T. Niinikoski, Nucl. Instrum. Meth. A **224**, 83 (1984).
[25] A. Giuliani, J. Low Temp. Phys. **167**, 991 (2012).
[26] D. Poda and A. Giuliani, Int. J. Mod. Phys. A **32**, 1743012 (2017).
[27] C. Alduino *et al.* (CUORE), Phys. Rev. Lett. **120**, 132501 (2018).
[28] D. Q. Adams *et al.* (CUORE), Phys. Rev. Lett. **124**, 122501 (2020).
[29] S. Pirro *et al.*, Phys. Atom. Nucl. **69**, 2109 (2006).
[30] T. Tabarelli de Fatis, Eur. Phys. J. C **65**, 359 (2010).
[31] A. Giuliani *et al.*, Eur. Phys. J. C **78**, 272 (2018).
[32] O. Azzolini *et al.* (CUPID-0), Eur. Phys. J. C **79**, 583 (2019).
[33] O. Azzolini *et al.* (CUPID-0), Phys. Rev. Lett. **123**, 032501 (2019).
[34] V. Alenkov *et al.* (AMoRE), Eur. Phys. J. C **79**, 791 (2019).
[35] E. Armengaud *et al.* (LUMINEU), Eur. Phys. J. C **77**, 785 (2017).
[36] D. V. Poda *et al.* (LUMINEU), AIP Conf. Proc. **1894**, 020017 (2017).
[37] E. Armengaud *et al.* (CUPID-Mo), Eur. Phys. J. C **80**, 44 (2020).
[38] S. Rahaman *et al.*, Phys. Lett. B **662**, 111 (2008).
[39] V. D. Grigorieva *et al.*, J. Mat. Sci. Eng. B **7**, 63 (2017).
[40] R. Arnold *et al.* (NEMO-3), Phys. Rev. D **92**, 072011 (2015).
[41] E. E. Haller, Infrared Phys. Techn. **35**, 127 (1994).
[42] E. Armengaud *et al.* (EDELWEISS), J. Instrum. **12**, P08010 (2019).
[43] L. Hehn *et al.* (EDELWEISS), Eur. Phys. J. C **76**, 548

(2016).
[44] C. Alduino *et al.* (CUORE), Phys. Rev. C **93**, 045503 (2016).
[45] O. Azzolini *et al.* (CUPID-0), Eur. Phys. J. C **78**, 734 (2018).
[46] B. Schmidt *et al.* (CUPID-Mo), J. Phys.: Conf. Ser. **1468**, 012129 (2020).
[47] S. Di Domizio, F. Orio, and M. Vignati, J. Instrum. **6**, P02007 (2011).
[48] R. Huang *et al.* (CUPID-Mo), arXiv:2010.04033.
[49] B. Schmidt *et al.* (EDELWEISS), Astropart. Phys. **44**, 28 (2013).
[50] R. Arnold *et al.* (NEMO-3), Eur. Phys. J. C **79**, 440 (2019).
[51] E. Armengaud *et al.* (CUPID-Mo), Eur. Phys. J. C **80**, 674 (2020).
[52] C. Alduino *et al.* (CUORE-0), Eur. Phys. J. C **77**, 13 (2017).
[53] C. Alduino *et al.* (CUORE), Eur. Phys. J. C **77**, 543 (2017).
[54] A. Caldwell, D. Kollár, and K. Kröninger, Comput. Phys. Commun. **180**, 2197 (2009).
[55] B. A. Faddegon *et al.*, Medical Physics **35**, 4308 (2008).
[56] L. Pandola, C. Andenna, and B. Caccia, Nucl. Instrum. Meth. A **350**, 41 (2015).
[57] J. Kotila and F. Iachello, Phys. Rev. C **85**, 034316 (2012).
[58] M. Mirea, T. Pahomi, and S. Stoica, Rom. Rep. Phys. **67**, 872 (2015).
[59] P. K. Rath *et al.*, Phys. Rev. C **88**, 064322 (2013).
[60] F. Šimkovic, V. Rodin, A. Faessler, and P. Vogel, Phys. Rev. C **87**, 045501 (2013).
[61] N. L. Vaquero, T. R. Rodríguez, and J. L. Egido, Phys. Rev. Lett. **111**, 142501 (2013).
[62] J. Barea, J. Kotila, and F. Iachello, Phys. Rev. C **91**, 034304 (2015).
[63] J. Hyvärinen and J. Suhonen, Phys. Rev. C **91**, 024613 (2015).
[64] L. S. Song, J. M. Yao, P. Ring, and J. Meng, Phys. Rev. C **95**, 024305 (2017).
[65] F. Šimkovic, A. Smetana, and P. Vogel, Phys. Rev. C **98**, 064325 (2018).
[66] P. K. Rath, R. Chandra, K. Chaturvedi, and P. K. Raina, Front. in Phys. **7**, 64 (2019).
[67] W. R. Armstrong *et al.* (CUPID Interest Group), CUPID pre-CDR, arXiv:1907.09376.